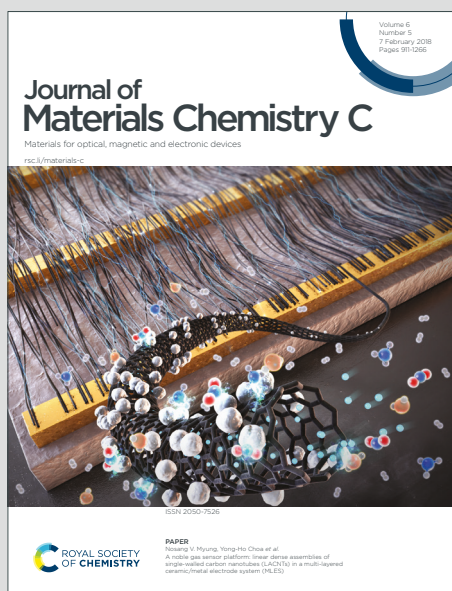


Journal of Materials Chemistry C

Materials for optical, magnetic and electronic devices

Accepted Manuscript

This article can be cited before page numbers have been issued, to do this please use: G. A. Valdivia, K. C. Kenney, E. W. Jackson, J. Bloxham, A. X. Wayment, D. J. Brock, S. J. Smith, J. Johnson and D. J. Michaelis, *J. Mater. Chem. C*, 2020, DOI: 10.1039/D0TC01829E.



This is an Accepted Manuscript, which has been through the Royal Society of Chemistry peer review process and has been accepted for publication.

Accepted Manuscripts are published online shortly after acceptance, before technical editing, formatting and proof reading. Using this free service, authors can make their results available to the community, in citable form, before we publish the edited article. We will replace this Accepted Manuscript with the edited and formatted Advance Article as soon as it is available.

You can find more information about Accepted Manuscripts in the [Information for Authors](#).

Please note that technical editing may introduce minor changes to the text and/or graphics, which may alter content. The journal's standard [Terms & Conditions](#) and the [Ethical guidelines](#) still apply. In no event shall the Royal Society of Chemistry be held responsible for any errors or omissions in this Accepted Manuscript or any consequences arising from the use of any information it contains.

6MNEP: A molecular cation with large hyperpolarizability and promising for nonlinear optical applications

[View Article Online](#)

DOI: 10.1039/D0TC01829E

Gabriel A. Valdivia-Berroeta, Karissa C. Kenney, Erika W. Jackson, Joseph Bloxham, Adam X. Wayment, Daniel J. Brock, Stacey J. Smith, Jeremy A. Johnson,[#] David J. Michaelis*

Department of Chemistry and Biochemistry, Brigham Young University, Provo, UT
84602

[#]jjohnson@chem.byu.edu

*dmichaelis@chem.byu.edu

Abstract

Molecular organic crystals are strategically designed for nonlinear optical applications using push-pull chromophores as the core feature. In this approach, electron-donating and accepting groups are connected through a π -conjugated bridge to obtain planar molecules with high hyperpolarizability. However, the non-centrosymmetric packing that is required for nonlinear optical (NLO) applications is a critical challenge that must be addressed to design useful materials. In this article, we present the new organic cation 6MNEP that shows a large hyperpolarizability and can be crystallized in ideal non-centrosymmetric structures for NLO applications, when paired with T and 4NBS anions. The 6MNEP cation was obtained by extending the conjugation length of already existing chromophores. We compare the 6MNEP crystals with other crystals that also have cations with extended conjugation lengths, but result in centrosymmetric crystal structures. Using the effective hyperpolarizability, we found 6MNEP-T and 6MNEP-4NBS to have 1.6 to 2.5 times larger macroscopic nonlinearities than benchmark NLO organic crystals. Additionally, the significantly lower absorption wavelength compared with other state-of-the-art crystals make 6MNEP-T and 6MNEP-4NBS promising materials for NLO applications like intense terahertz generation.

1. Introduction

Many non-centrosymmetric organic crystals have been studied for nonlinear optical (NLO) applications such as second-harmonic (SHG),¹ sum-frequency (SFG),² and terahertz (THz) generation.³ These types of NLO materials can feature ultrafast response times,⁴ large second-order susceptibilities,⁵ and the possibility of incorporating different functional groups to improve the NLO activity.⁶ In order to create efficient NLO crystals, highly conjugated and polar organic molecules can be optimized to have large molecular hyperpolarizabilities. In addition, organic molecules must exhibit non-centrosymmetric packing in the crystalline state, which is required for NLO activity.⁷

Push-pull chromophores suitable for NLO applications are designed by connecting electron-donating (**ED**) with electron-accepting (**EA**) groups using a π -conjugated aromatic bridge (**Bd**), as seen in **Figure 1**. For instance, the DAS cation in the stilbazolium crystal DAST (4-dimethylamino-N-methyl-4-stilbazolium tosylate) features a dimethyl amino **ED** group connected through a styryl bridge (**Bd**) to a pyridinium **EA** moiety (**Figure 1a**).⁸ Hydrogen bonding **ED** groups such as hydroxyl⁹ and methoxy¹⁰ have also been employed in fabricating push-pull molecules (**Figure 1b**). On the other side of the bridge, **EA** groups such as pyridinium,⁸ quinolinium,¹¹ and indolinium¹² have found widespread application in NLO material design.

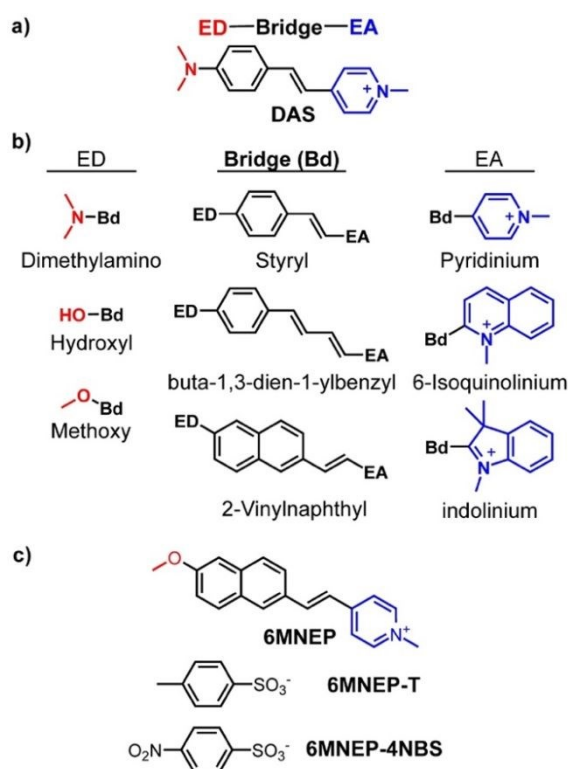


Figure 1 a) Push-pull chromophore design using electron donating (**ED**), bridging (**Bd**), and electron accepting (**EA**) groups, as seen in DAST. **b)** Common examples of **ED**, **Bd**, and **EA** groups. **c)** 6MNEP-T and 6MNEP-4NBS molecular structures.

An ideal NLO organic crystal combines a chromophore exhibiting large molecular hyperpolarizability with non-centrosymmetric packing in the crystalline state. However, different conformations can be observed for organic chromophores. The ideal scenario for NLO applications is to have the molecules arranged in a non-centrosymmetric, head-to-tail conformation.¹³ To quantify this, an order parameter has been defined that corresponds to the cosine cubed of the angle between the hyperpolarizability vector and the polar axis of the crystal ($\cos^3(\theta_p)$).¹⁴ For centrosymmetric crystals, this angle is 90° , and therefore the order parameter and the effective hyperpolarizability are both 0. For non-centrosymmetric crystals, the order parameter value will be closer to 1 if the chromophores are aligned in an ideal head-to-tail conformation. Due to the difficulty of predicting solid-state arrangements for push-pull chromophores, usually the molecular hyperpolarizability is optimized and then slight modifications are introduced to induce non-centrosymmetric molecular packing.¹²

A common approach to increase hyperpolarizability (β), while keeping the **ED** and **EA** groups unchanged (see **Figure 1a**), is to increase the π -conjugation length. Using this strategy, the bis-alkene derivative of DAST, DACSC (4-((1E,3E)-4-(4-(dimethylamino)phenyl)buta-1,3-dien-1-yl)-1-methylpyridin-1-ium 4-chlorobenzene sulfonate),¹⁵ was recently designed and characterized (**Figure 2**). Crystals incorporating the DASC cation show the required non-centrosymmetric packing; however, they co-crystallize with water and have sub-optimal cation alignment.

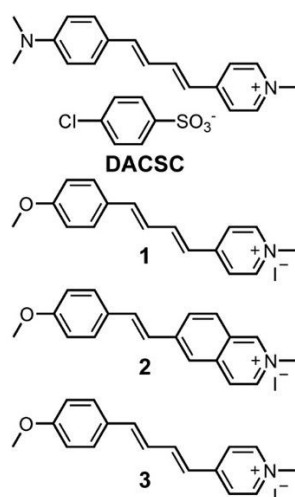


Figure 2 DACSC molecular structure and extended conjugation molecules developed by Ajito *et al* (**1-3**).

Figure 2 also shows chromophores designed by Tsuji *et al.* with methoxy **ED** groups and extended conjugation lengths using either (E)-buta-1,3-dien-1-ylbenzyl (**1**, **3**) or styryl (**2**) bridges connected to pyridinium (**1**, **3**) or 6-isoquinolinium (**2**) **EA** moieties.¹⁶ Improved β values along with reduced maximum absorption wavelengths were found for the fused-ring molecules (**2**). Despite the good characteristics of these π -extended systems, crystal structures

were not reported and only qualitative second-harmonic generation tests were performed to prove the NLO activity of the chromophores.¹⁶

To compare the macroscopic nonlinearities for several organic NLO compounds, we use the effective hyperpolarizability (β_{iii}^{eff}) that corresponds to the product of the molecular β with the order parameter. This parameter has been shown to correlate strongly with measured NLO properties like SHG and THz generation.^{11, 17-19} **Table 1** shows the reported order parameter and effective hyperpolarizability values for benchmark organic NLO crystals DAST¹⁸ and HMQ-TMS (2-(4-hydroxy-3-methoxystyryl)-1-methylquinolinium 2,4,6-trimethylbenzenesulfonate),¹⁹ as well as HMQ-T (2-(4-hydroxy-3-methoxystyryl)-1-methylquinolinium 4-methylbenzenesulfonate)¹¹ and OHP-CBS (4-(4-hydroxystyryl)-1-methylpyridinium 4-chlorobenzenesulfonate).¹⁷ Due to its large molecular hyperpolarizability and optimal molecular packing, HMQ-TMS has the largest effective hyperpolarizability of these benchmark crystals.

Table 1 Order parameter ($\cos^3(\theta_p)$), DFT calculated effective hyperpolarizability (β_{iii}^{eff}), and powder second harmonic measurements relative to DAST for organic nonlinear optical crystals. β_{iii}^{eff} correlates strongly with NLO properties like second harmonic generation and THz generation.^{11, 19}

Property/ Chromophore	Order parameter ($\cos^3(\theta_p)$)	β_{iii}^{eff} (10^{-30} esu)	Powder SHG
DAST ^{11, 18}	0.83	161	1.0
HMQ-TMS ¹⁹	1.0	185	-
HMQ-T ¹¹	0.91	155	0.77
OHP-CBS ¹⁷	1.0	118	0.36
6MNEP-T	0.97	297	-
6MNEP-4NBS	0.97	292	-

In this article, we introduce 6MNEP, a cationic push-pull chromophore. This cation features a methoxy ED group connected to a pyridinium EA group through a 2-vinylnaphthyl bridge. When this organic cation is combined with T and 4NBS anions, as shown in **Figure 1c**, it produces crystals with large molecular hyperpolarizability and ideal non-centrosymmetric packing in the crystalline state. We also report the synthesis and X-ray structure determination of other four centrosymmetric molecular cations with π -extended conjugation length and compare them with 6MNEP-T and 6MNEP-4NBS.

2. Results and discussions

2.1 Chromophores design

To design the π -extended chromophores, methoxy and dimethyl amino ED groups were combined with (E)-buta-1,3-dien-1-ylbenzyl and 2-vinylnaphthyl π -extended bridges in conjunction with pyridinium and 6-isoquinolinium EA groups to yield unique cations, as shown in **Figure 3**. The methoxy derivatives 6MNEP, MBDM, and 6MEIQ along with

dimethyl amino-functionalized chromophores 6DMIQ and DACS were paired with T (p-toluenesulfonate) and 4NBS (4-nitrobenzenesulfonate) anions to form organic salts. In order to compare the molecular hyperpolarizability of the designed π -extended chromophores, *ab-initio* calculations in the gas phase were performed for all the compounds.²⁰ The β_{gas} value of state-of-the-art DAST cation (**Figure 1a**) was also computed and utilized as reference. Geometry optimization and single-point hyperpolarizability calculations were performed, as explained in the experimental section. β_{gas} values were found to be 286 (6MNEP), 243 (MBDM), 299 (6MEIQ), 394 (6DMIQ), and 282 (DACS) $\times 10^{-30}$ esu. These values are from 1.56 to 2.52 times higher compared to the β obtained for the DAS cation (155×10^{-30} esu). These results confirm the positive impact of π -extended systems on the molecular hyperpolarizability.

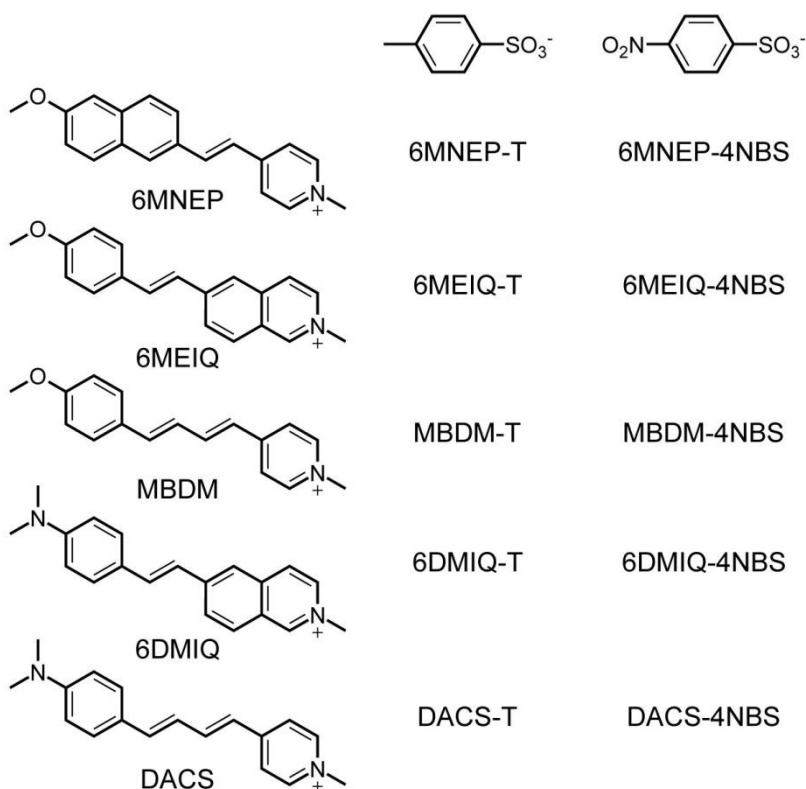


Figure 3 Molecular structures of π -extended chromophores. From top to bottom, 6MNEP, 6MEIQ, MBDM, 6DMIQ, and DACS paired with T and 4NBS anions

Out all of the designed cations, 6MNEP was the only one that showed ideal head-to-tail conformations for NLO applications when combined with T and 4NBS anions. As shown in **Table 1**, combining the ideal molecular packing in the crystalline state with the large hyperpolarizability values obtained from single-crystal structure coordinates, 6MNEP-T and 6MNEP-4NBS show effective hyperpolarizability values from 1.6 to 2.5 times higher compared with state-of-the-art organic crystals.

2.1 X-ray crystal structures analysis

View Article Online
DOI: 10.1039/D0TC01829E

To evaluate the molecular packing of the featured organic salts, the different cations were synthesized with 4-methyl (T) and 4-nitro (4NBS) benzene sulfonate anions, and single crystals were grown via slow evaporation techniques. **Figure 4** shows the crystal structures obtained via X-ray diffraction experiments for 6MNEP, 6MEIQ, and MBDM. Arrows from ED to EA groups are drawn to indicate parallel and antiparallel arrangements. Lattice and refinement parameters for the obtained crystal structures are detailed in the Support Information. As observed in **Figure 4**, 6MNEP-T and 6MNEP-4NBS feature similar molecular packing and the same triclinic P1 space group with nearly perfect alignment for NLO applications. Other chromophores with known NLO activity, such as DSNS and OHP-CBS,^{17, 21} have crystallized in the same space group. As shown in **Figure S2**, 6MNEP was also paired with 3NBS (3-nitrobenzenesulfonate) and 4TFS (4-(trifluoromethyl)benzenesulfonate) anions, however the 3NBS derivative is centrosymmetric and the 4TFS compound, while non-centrosymmetric, features sub-optimal molecular packing.

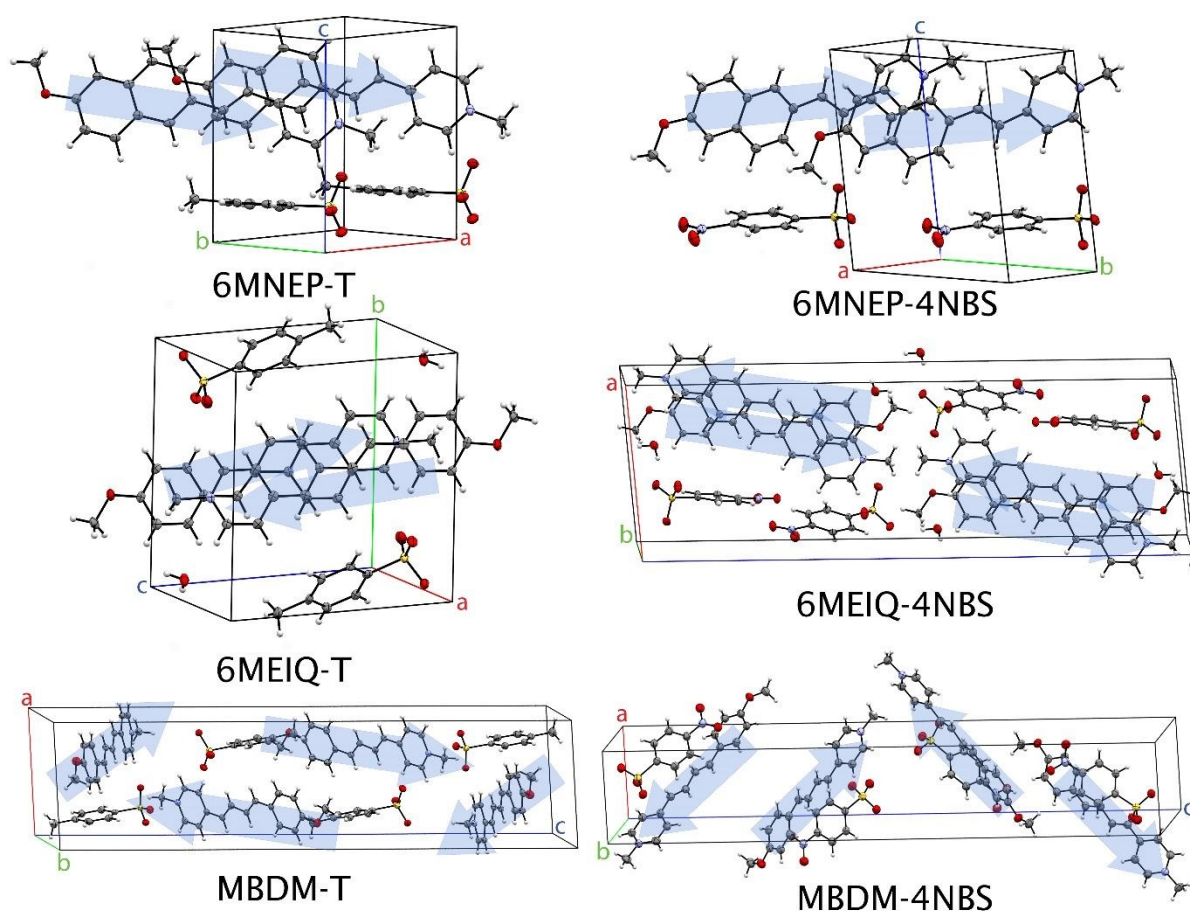


Figure 4 Crystal structures of π -extended methoxy derivatives. Blue arrows point from ED to EA groups and indicate parallel (6MNEP) and antiparallel (MBDM, 6MEIQ) packing.

Similar to 6MNEP, 6MEIQ also features a fused ring system with extended conjugation. However, solvent molecules were co-crystallized with 6MEIQ in the solid state. This could

explain the centrosymmetric molecular packing obtained for 6MEIQ-T and 6MEIQ-4NBS (see **Figure 4**). In order to eliminate these crystallized solvent molecules, the methyl attached to the quaternary isoquinolinium nitrogen was replaced by an ethyl group. **Figure S3** shows the molecular packing of 6MEIQE-4NBS with no co-crystallized solvent molecules, but the molecular packing maintains its centrosymmetric alignment. On the other hand, the bisalkene chromophore MBDM crystallizes in the centrosymmetric monoclinic space group $P2_1/c$ when combined with the T anion, while MBDM-4NBS features a $P2_12_12_1$ non-centrosymmetric space group, as observed at the bottom of **Figure 4**. Despite the acentric nature of the orthorhombic MBDM-4NBS crystal, the arrangement of the molecular cations is antiparallel, and therefore we expect no NLO activity. **Figure S2c** shows the molecular packing of MBDM-N2S (N2S = 2-naphthalenesulfonate), which also forms a centrosymmetric arrangement. In order to induce head-to-tail relative conformations, the methyl moiety in the quaternary nitrogen of MBDM was substituted for an ethyl group. As shown in **Figure S4**, similar conformations with non-centrosymmetric space groups, but poor molecular alignment, were obtained for the ethylated compounds when combined with 3NBS, 4NBS, N2S, and CBS (4-chlorobenzenesulfonate).

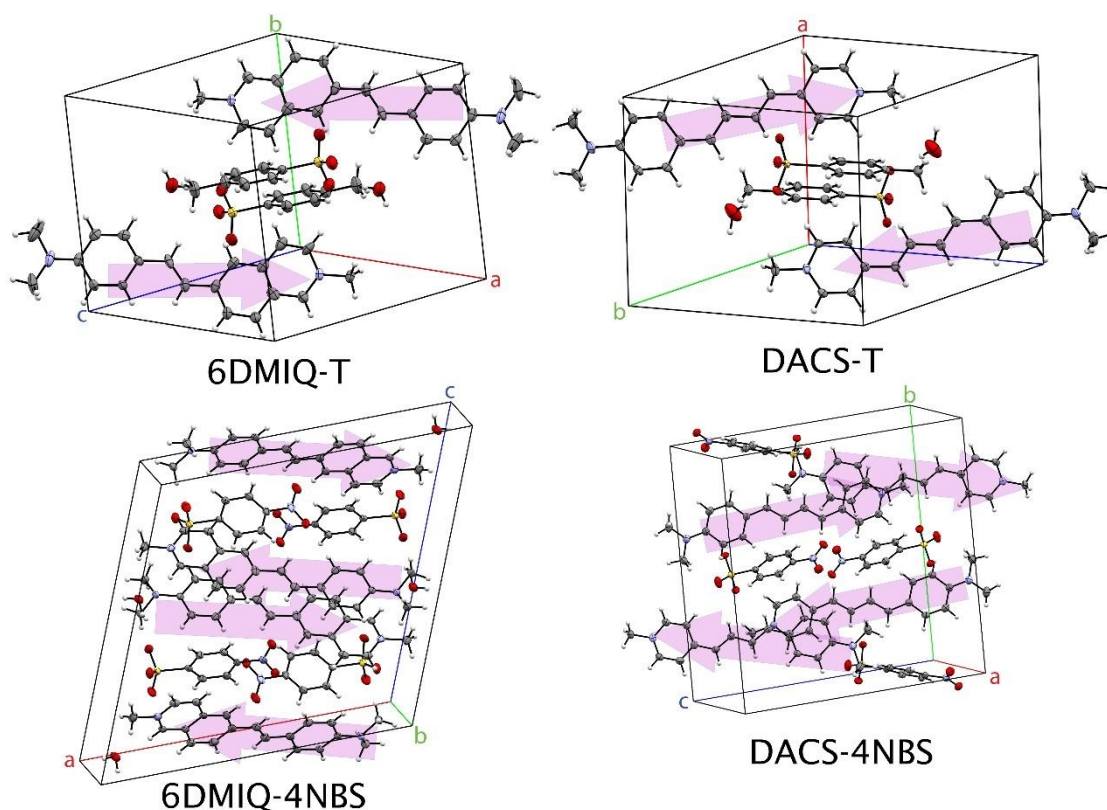


Figure 5 Crystal structures of π -extended dimethylamino derivatives. Pink arrows go from ED to EA groups and indicate parallel and antiparallel packing.

As shown in **Figure 5**, all the chromophores with dimethylamino ED groups (6DMIQ, DACS) feature centrosymmetric space groups. Other organic crystals with dimethylamino groups (DAST and 4DEP) have been shown to form centrosymmetric packing when co-crystallized water molecules are present.²² However, DACS-4NBS does not show any co-crystallized water

molecules, and the observed molecular packing is still centrosymmetric. In order to eliminate the water molecules from the 6DMIQ crystals, the cation was modified with an N-ethyl group instead of a methyl group on the isoquinolinium nitrogen. The crystal structures for the ethylated molecular cation paired with different anions are shown in **Figure S5**. Even though co-crystallized water molecules are not present, the molecular packing is still centrosymmetric and, therefore, NLO inactive.

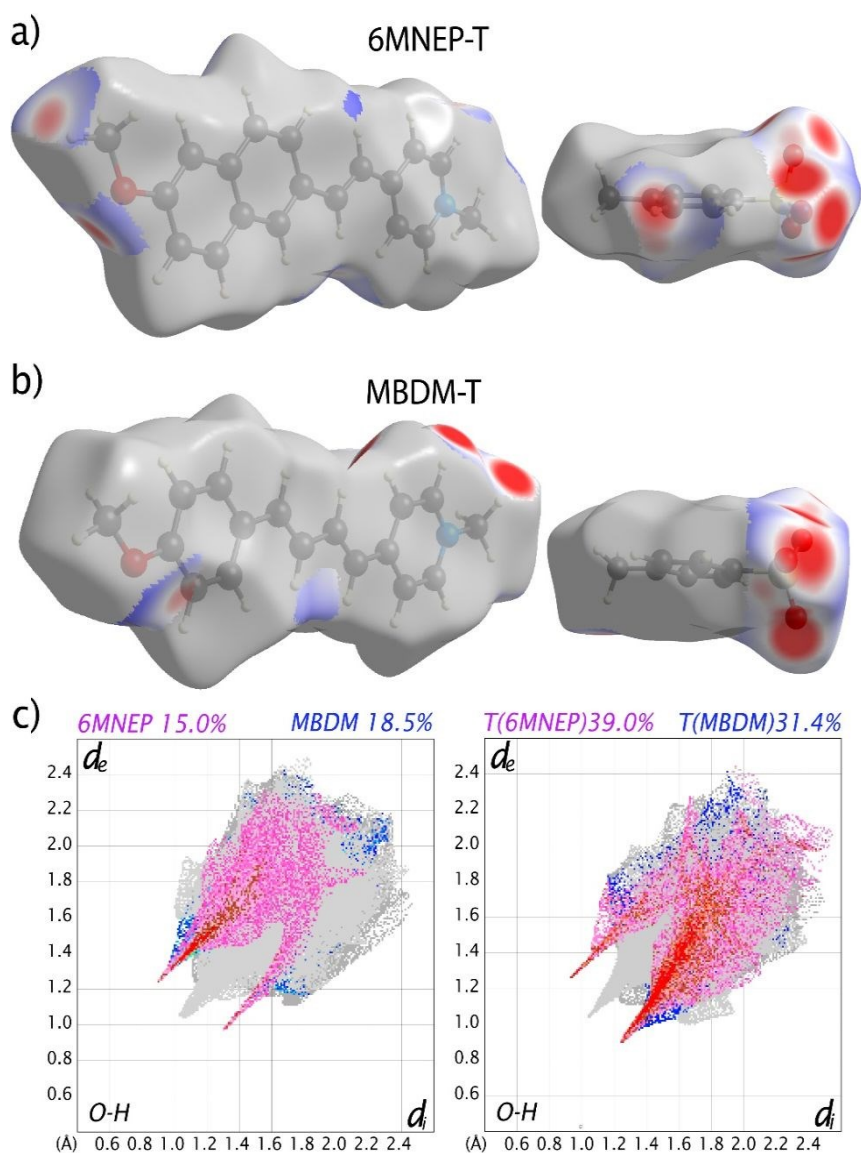


Figure 6 Hirshfeld surfaces of a) 6MNEP-T and b) MBDM-T. c) Fingerprint plots for O-H intermolecular interactions present in 6MNEP-T (pink) and MBDM-T (blue)

As we see above, 6MNEP shows optimal molecular packing, and therefore we examined the crystal structure of 6MNEP-T in more detail and compared it with MBDM-T. As shown in **Figure 4**, 6MNEP-T features parallel relative conformations in contrast to antiparallel packing observed in MBDM-T. The drastic differences in molecular packing observed in methoxy functionalized chromophores could be attributed to the presence of an extra aromatic ring in the **ED** side of 6MNEP. The increased Van der Waals volume induced by the extra ring in

6MNEP could be responsible for the favorable interactions in the crystalline state that induce the head-to-tail conformations. However, similar conformations were not observed in 6MEIQ, which also features an extra aromatic ring compared to MBDM. This is mainly due to the presence of co-crystallized solvent molecules, and therefore correlations between one extra aromatic ring and non-centrosymmetric packing are impossible to establish.

To characterize specific intermolecular interactions in 6MNEP-T and MBDM-T that could help explain the drastic differences in molecular packing, we calculated Hirshfeld surfaces, as explained in the method sections. **Figure 6a-b** shows the Hirshfeld surfaces of 6MNEP-T and MBDM-T, normalized to the atomic Van der Waals volumes, characterizing O-H intermolecular interactions. As observed in **Figure 6c**, 6MNEP-T features overall shorter interaction distances compared with MBDM-T. This difference is explained by strong cation-anion interactions between the **ED** methoxy group and the methyl attached to the quaternary nitrogen of the **EA** moiety. As seen in **Figure 6b**, this same interaction is not observed in MBDM-T and appears to be responsible for the ideal alignment observed in 6MNEP chromophores.

2.1.1 Molecular alignment stabilities for 6MNEP-T

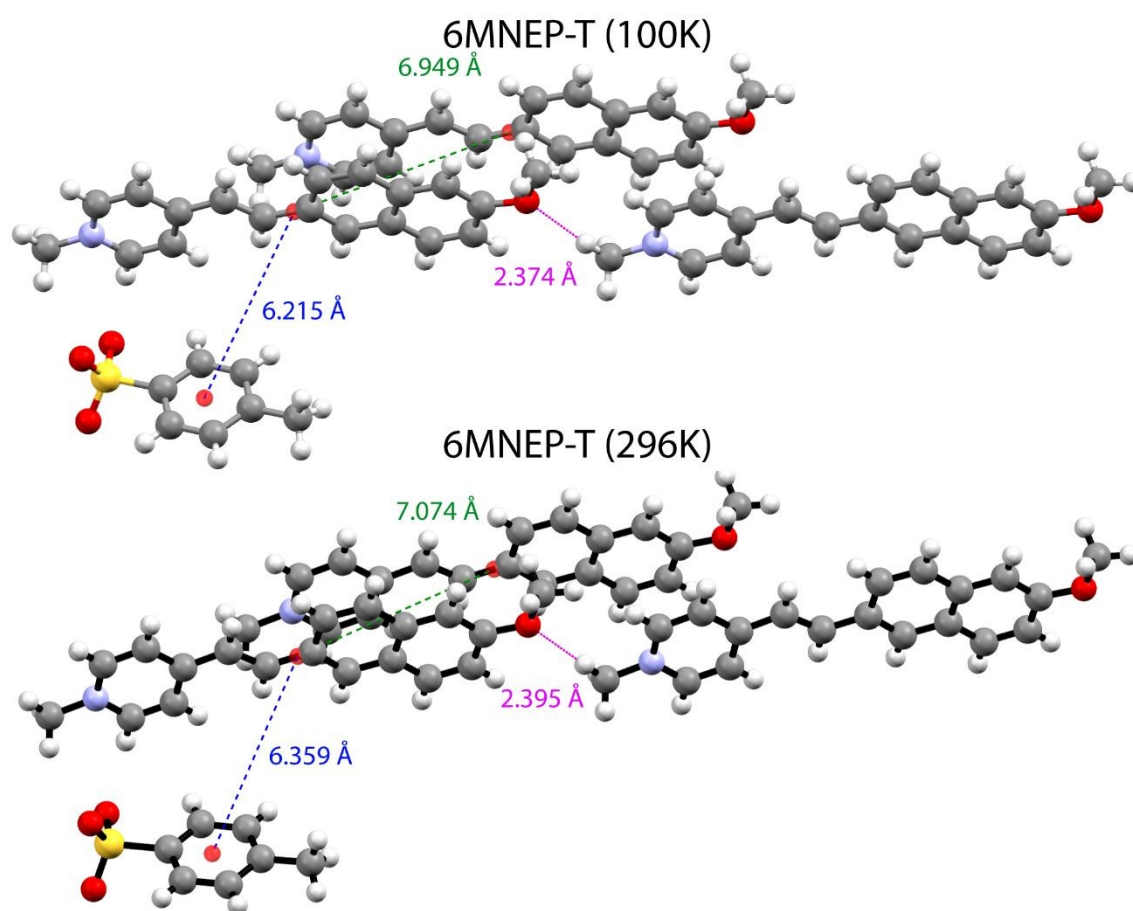


Figure 7 Intermolecular distances for 6MNEP-T crystal structures at 100 and 296 K.

Organic NLO crystals are utilized in applications involving high-power lasers; therefore, the stability of the parallel molecular alignments for 6MNEP chromophores in the crystalline state must be evaluated. X-ray diffraction data shows the same crystal structure for 6MNEP-T at 100 and 296 K (see Supporting Information), with small differences due to thermal expansion. In addition, intermolecular distances analysis reveals similar cation-cation and anion-anion distances at both temperatures, as observed in **Figure 7**.

2.2 Hyperpolarizability calculations and NLO properties estimation

To evaluate the applicability of 6MNEP-T and 6MNEP-4NBS as potential NLO crystals, the effective hyperpolarizability, $\beta_{iii}^{eff} = \beta_{tot} \cos^3(\theta_p)$, was calculated.⁴ This parameter is also known as the macroscopic optical nonlinearity, and it has been extensively used to compare between different organic NLO crystals showing a high correlation with experimental SHG measurements.^{11, 19} In this study, β_{tot} was obtained from DFT calculations using the measured crystal atomic coordinates. The order parameter ($\cos^3(\theta_p)$) was calculated from the angle between β and the *ac*-crystallographic plane, as depicted in **Figure 8**. In **Table 1**, we compare the values of β_{iii}^{eff} for 6MNEP-T and 6MNEP-4NBS with state-of-the-art organic salt crystals, namely, HMQ-TMS,¹⁹ HMQ-T,¹¹ DAST,¹⁸ and OHP-CBS.¹⁷ Significantly improved β_{iii}^{eff} values are observed for 6MNEP-T and 6MNEP-4NBS, ranging from 1.6 to 2.5 times higher when compared with HMQ-TMS and OHP-CBS, respectively. Powder SHG test results are also included, where available, to show the positive correlation between β_{iii}^{eff} and the experimental determinations. It is important to note that phase-matching conditions are not considered in SHG experiments or β_{iii}^{eff} calculations. To the best of our knowledge, the calculated β_{iii}^{eff} values for 6MNEP-T and 6MNEP-4NBS are the highest ones reported so far in the literature.

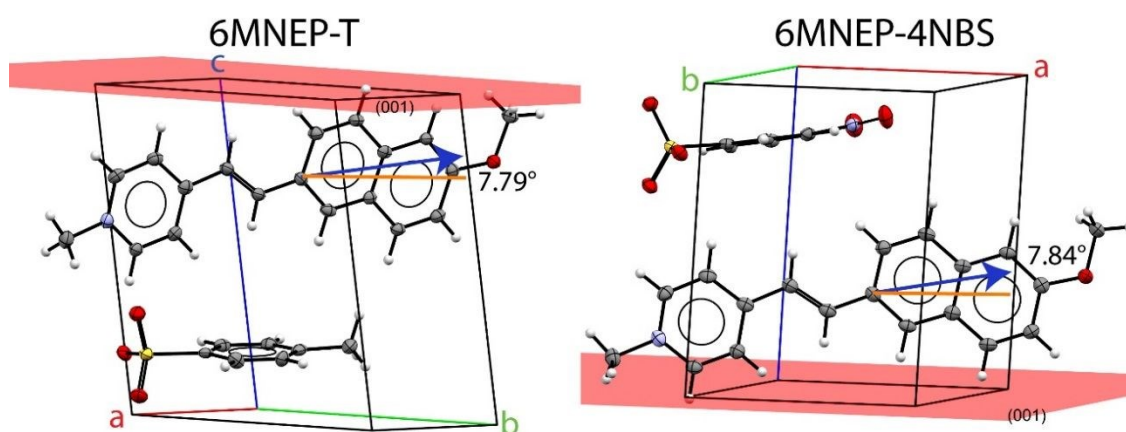


Figure 8 Angle between the molecular hyperpolarizability (blue) and the polar axis (red) for a) 6MNEP-T, and b) 6MNEP-4NBS.

To further confirm the second-order nonlinearity estimations obtained with β_{iii}^{eff} , we decided to perform additional calculations, including two and four cations in the gas phase, and frequency-dependent hyperpolarizabilities studies in methanol solution using the polarizable continuum model (PCM). Conformations employed for two and four cations calculations are

shown in **Figure S7**, and the obtained β_{tot} results compared with other NLO organic crystals are shown in **Table 2**. 6MNEP chromophores exhibit values from 1.4 to 2.8 times higher than DAST, HMQ-TMS, HMQ-T, and OHP-CBS for all the configurations analyzed. More importantly, our calculations reflect the sub-optimal order parameter of DAST, which shows a β_{tot} of 0.89 times the expected value for a four cations arrangement. This reduced β_{tot} determination obtained for DAST strongly contrasts with the ideal values obtained for 6MNEP salts, where no lessening of the hyperpolarizability was observed for 6MNEP-T, and only a 4% reduction was determined for the 6MNEP-4NBS four cations calculations.

Table 2 One, two, and four cation calculations for DAST, HMQ-TMS, HMQ-T, OHP-CBS, 6MNEP-T, and 6MNEP-4NBS. Calculations were performed using the B3LYP/NLO-V configuration. Molecular arrangements employed to calculate the β_{tot} values are shown in **Figure S7** and were obtained from X-ray coordinates as deposited in the CCDC database (See methods for CCDC IDs).

Configuration/ Chromophore	One cation β_{tot} (10^{-30} esu)	Two cations β_{tot} (10^{-30} esu)	Four cations β_{tot} (10^{-30} esu)
DAST	188	412	673
HMQ-TMS	209	470	838
HMQ-T	183	367	752
OHP-CBS	115	239	485
6MNEP-T	318	673	1288
6MNEP-4NBS	311	643	1194

Table 3 Polarizable continuum model calculations in methanol for DAST, HMQ-TMS, HMQ-T, OHP-CBS, 6MNEP-T, and 6MNEP-4NBS. Optimization and polar calculations were performed in methanol from 800 to 1900 nm using the B3LYP/NLO-V method. Frequency-dependent hyperpolarizability values, $\beta(-\omega;\omega;0)$, are reported in 10^{-30} esu units.

Chromophore/ Wavelength (nm)	DAST	HMQ- TMS	HMQ- T	OHP- CBS	6MNEP- T	6MNEP- 4NBS
800	521	474	467	306	668	668
900	524	477	470	307	672	672
1000	527	481	473	309	676	676
1100	531	485	477	310	681	681
1200	535	489	482	312	687	687
1300	540	494	486	314	693	693
1400	544	499	491	317	699	699
1500	550	505	497	319	707	707
1600	556	512	503	322	715	715
1700	562	519	510	325	724	723
1800	568	526	517	328	734	732
1900	576	534	525	331	743	743

Solution phase calculations in methanol were performed, as explained in the methods section. The $\beta(-\omega;\omega;0)$ values obtained for the studied organic NLO materials are shown in **Table 3**.

For the analyzed chromophores, a monotonic increase in the β_{tot} values with respect to the wavelength was observed. This is an indication of the absence of important absorption effects in the analyzed wavelength range. From 800 to 1900 nm, 6MNEP-T and 6MNEP-4NBS outperform the other NLO organic materials. However, the improvement for 6MNEP chromophores is lower compared with $\beta_{\text{iii}}^{\text{eff}}$ and two or four cations calculations. The enhancement factor for 6MNEP-T and 6MNEP-4NBS in frequency-dependent calculations corresponds from 1.3 to 2.2 times compared to DAST and OHP-CBS, respectively. Despite the lower improvement factors observed for 6MNEP materials in solution phase calculations in methanol compared with other NLO organic crystals, 6MNEP-T and 6MNEP-4NBS still display higher nonlinearities compared with DAST, HMQ-TMS, HMQ-T, and OHP-CBS.

2.3 Crystal and optical properties

Table 4 Wavelength of maximum absorption (λ_{max}) in methanol solution, transparency range cut-off in the crystalline state, and melting point for 6MNEP-T, 6MNEP-4NBS, HMQ-TMS, HMQ-T, DAST, and OHP-CBS.

Property/ Chromophore	λ_{max} (nm)	Transparency cut-off (nm)	Melting point (°C)
DAST ¹⁸	475	595	256
HMQ-TMS ¹⁹	439	680	274
HMQ-T ¹¹	439	595	273
OHP-CBS ¹⁷	390	490	~270
6MNEP-T	399	475	224
6MNEP-4NBS	399	-	234

An important consideration in designing organic NLO crystals is to keep the wavelength of maximum absorption (λ_{max}) shifted to values < 410 nm to avoid two-photon absorption processes that occur when the crystals are irradiated with high-power lasers. A common system employed to pump these NLO crystals is the Ti:Sapphire laser with a central wavelength of 800 nm. As observed in **Table 4**, the λ_{max} values for 6MNEP-T, 6MNEP-4NBS, HMQ-TMS, HMQ-T, DAST, and OHP-CBS are 399, 399, 439, 439, 475, and 390 nm, respectively. Therefore, the likelihood of getting two-photon absorption damage in HMQ-TMS, HMQ-T, or DAST crystals when pumped with a Ti:Sapphire system is higher compared with 6MNEP-T and 6MNEP-4NBS crystals. On the other hand, OHP-CBS features a lower λ_{max} value of only 9 nm less when compared with the 6MNEP salts. However, the $\beta_{\text{iii}}^{\text{eff}}$ parameter is 2.5 times greater for the newly designed chromophores. Similar trends, as obtained in solution, are observed for transparency cut-off parameters with 6MNEP-T and OHP-CBS having lower values with respect to the other featured crystals and below 500 nm. Another critical advantage of OHP-CBS is related to improved phase-matching conditions in the THz region, that have been attributed to the yellow color of OHP-CBS crystals, compared with orange or red crystals such as HMQ-T and DAST. Both 6MNEP-T and 6MNEP-4NBS exhibit yellow-colored crystals as it is confirmed by the λ_{max} of 399 nm, and therefore good phase-matching conditions in the THz region are expected. Finally, melting point data reveal similar stability for 6MNEP salts compared with benchmark NLO organic crystals, as detailed in **Table 4**.

Slow evaporation and slow-cooling methods with different organic solvents are currently being tested to grow large crystals of 6MNEP-T and 6MNEP-4NBS. To date, only polycrystalline solids have been obtained, as confirmed by XRD experiments. Similar crystallization problems have been reported for the nonlinear crystal DSNS (4-dimethylamino-N-methyl-4-stilbazolium naphthalene-2-sulfonate),²¹ however, a study from Guan *et al.* showed the possibility of growing DSNS nanowires with detectable SHG activity.²³ We propose that 6MNEP compounds can be utilized for similar applications, and we are currently pursuing these efforts.

3. Conclusions

Chromophores with π -extended conjugation lengths were synthesized and crystal structures reported for 6MNEP, MBDM, 6MEIQ, 6DMIQ, and DACS with T and 4NBS anions. Despite the improved β values for these chromophores, only compounds containing 6MNEP cations crystallized with nearly perfect alignment for NLO applications. The β_{iii}^{eff} parameters of 6MNEP-T and 6MNEP-4NBS were from 1.6 to 2.5 times higher compared with state-of-the-art NLO organic crystals. Work is currently underway to produce large-high-quality crystals optimal for NLO applications.

4. Experimental Section

Synthesis and NMR characterization: 6MNEP, MBDM, and DACS organic salts were synthesized by a condensation reaction at room temperature between the 1,4-dimethyl pyridinium sulfonate salts and the corresponding aldehydes in the presence of piperidine as the catalyst. 6DMIQ and 6MEIQ derivatives were obtained by Wittig reaction of the corresponding benzaldehydes to obtain N,N-dimethyl- and 4-methoxy- 4-vinylaniline. The vinyl compound was reacted with 6-bromoisoquinoline with Pd(OAc) as catalyst to obtain the 6DMIQ and 6MEIQ cation precursors. Anions were added by alkylation reactions in toluene. Additional details about the reaction procedures, yields, and NMR data are provided in the Supporting Information.

Calculations: Density functional theory calculations were performed using the Gaussian 09 software. The B3LYP functional, along with the 6-311++G** basis set, were employed to optimize molecular geometries and then find the β tensor components. This configuration was selected due to the extensive validation presented in the literature with other NLO organic materials. In addition, we performed a calculation optimization study with different DFT and semi-empirical methods; the obtained results are presented in the Supporting Information (See **Table S1**). The total magnitude of β was calculated using the following equations:

$$\beta_i = \sum_j (\beta_{ijj} + \beta_{jij} + \beta_{jji}) \quad \text{Eq. 1a}$$

$$\beta_{tot} = \sqrt{\beta_x^2 + \beta_y^2 + \beta_z^2}$$

View Article Online
DOI: 10.1039/D0TC01829E

Eq 1b

Calculations with two and four cations were set up with the x-ray crystal coordinates for DAST (CCDC ID: 1175744), HMQ-TMS (CCDC ID: 931931), HMQ-T (CCDC ID: 824804), OHP-CBS (CCDC ID: 1586163), 6MNEP-T (CCDC ID: 1867834), 6MNEP-4NBS (CCDC ID: 1867835). Cations' conformations examples are provided in **Figure S7**. To facilitate the convergence of the calculations, the B3LYP/NLO-V method was employed.

Frequency-dependent calculations were performed by optimizing DAST, HMQ-T, HMQ-TMS, OHP-CBS, 6MNEP-T, and 6MNEP-4NBS in a methanol polarizable continuum model. The same solvent model was employed to run polar calculations for wavelengths from 800 to 1900 nm. Hyperpolarizability, $\beta(-\omega;\omega;0)$, values were obtained directly from the Gaussian 09 output.

X-ray crystallography: Small single crystals for X-ray diffraction experiments were obtained by slow evaporation of the compounds in methanol. The crystals were harvested in oil, mounted in a loop, and centered using a video camera. Diffraction data were collected using a Cu (K_{α} , 1.54178 Å) rotating anode as the X-ray source and a CCD camera as the detector. Diffraction peaks were integrated, scaled, and corrected using the APEX3 software package. Chemical structures were solved with the dual-space algorithm incorporated in SHELXT.²⁴ Refinement of the initial structural solutions was performed against F^2 on all data using least squares full-matrix strategy as it is included in SHELXL-2014.²⁵ Unit cell, and refinement parameters are reported in the Supporting Information.

Hirshfeld analysis: Hirshfeld surfaces were calculated using the Crystal Explorer software. Surfaces were calculated considering the atomic Van der Waals radius of the atoms inside the surface. Plots characterizing the inner atom – surface distances (d_i) and the outer atom – surface distances (d_e) were also generated.

Optical Characterization: UV-Vis absorption measurements were performed in a Carry 5e spectrometer using a 1-cm quartz cell and methanol as solvent. Data were collected from 300 to 500 nm, and the absorption intensity was normalized for comparison between chromophores. Absorption traces are shown in **Figure S6b**.

Transparency cut-off value determinations: Measurements were performed using a JASCO V-770 spectrometer using a 2nm data interval and 0.06 seconds response times. A large and highly twinned crystal of 6MNEP-T was utilized in the measurements. The obtained trace is shown in **Figure S6a**.

Differential Scanning Calorimetry: Melting points and heats of fusion were obtained with a TA Instruments Q2000 modulated differential scanning calorimeter (MDSC). The MDSC baseline was calibrated with sapphire disks and the thermocouples were calibrated using

ASTM method E967-08. This method measures melting points or phase transitions of indium, adamantane, water, tin, and lead to calibrate across the range 210 K to 600 K using a cubic spline. Using this calibration, experimental uncertainty in temperature is estimated to be much lower than 1%. A heating rate of 5°C/min was employed. DSC traces are shown in **Figure S8**.

New Article Online
DOI: 10.1039/C01829E

5. References

1. T. P. Radhakrishnan, *Accounts of Chemical Research*, 2008, **41**, 367-376.
2. M. Kitazawa, R. Higuchi, M. Takahashi, T. Wada and H. Sasabe, *Applied physics letters*, 1994, **64**, 2477-2479.
3. Z. Yang, L. Mutter, M. Stillhart, B. Ruiz, S. Aravazhi, M. Jazbinsek, A. Schneider, V. Gramlich and P. Günter, *Advanced Functional Materials*, 2007, **17**, 2018-2023.
4. S.-H. Lee, M. Jazbinsek, C. P. Hauri and O. P. Kwon, *CrystEngComm*, 2016, **18**, 7180-7203.
5. R. W. Boyd, *Nonlinear optics*, Elsevier, 2003.
6. H. S. Nalwa and S. Miyata, *Nonlinear optics of organic molecules and polymers*, CRC press, 1996.
7. S. H. Lee, B. J. Kang, J. S. Kim, B. W. Yoo, J. H. Jeong, K. H. Lee, M. Jazbinsek, J. W. Kim, H. Yun, J. Kim, Y. S. Lee, F. Rotermund and O.-P. Kwon, *Advanced Optical Materials*, 2015, **3**, 756-762.
8. P. Y. Han, M. Tani, F. Pan and X. C. Zhang, *Optics Letters*, 2000, **25**, 675-677.
9. F. D. J. Brunner, O. P. Kwon, S.-J. Kwon, M. Jazbinšek, A. Schneider and P. Günter, *Optics express*, 2008, **16**, 16496-16508.
10. F. D. J. Brunner, S.-H. Lee, O. P. Kwon and T. Feurer, *Optical Materials Express*, 2014, **4**, 1586-1592.
11. P. J. Kim, J. H. Jeong, M. Jazbinsek, S. B. Choi, I. H. Baek, J. T. Kim, F. Rotermund, H. Yun, Y. S. Lee and P. Günter, *Advanced Functional Materials*, 2012, **22**, 200-209.
12. G. A. Valdivia-Berroeta, E. W. Jackson, K. C. Kenney, A. X. Wayment, I. C. Tangen, C. B. Bahr, S. J. Smith, D. J. Michaelis and J. A. Johnson, *Advanced Functional Materials*, 2019, 1904786.
13. M. Jazbinsek, U. Puc, A. Abina and A. Zidansek, *Applied Sciences*, 2019, **9**, 882.
14. J. Zyss and J. L. Oudar, *Physical Review A*, 1982, **26**, 2028.
15. S. J. Sundaram, J. V. Ramaclus, P. Antony, M. Jaccob and P. Sagayaraj, *New Journal of Chemistry*, 2018, **42**, 18865-18872.
16. K. Tsuji, N. Nishimura, X.-M. Duan, S. Okada, H. Oikawa, H. Matsuda and H. Nakanishi, *Bulletin of the Chemical Society of Japan*, 2005, **78**, 180-186.
17. C. U. Jeong, B. J. Kang, S. H. Lee, S. C. Lee, W. T. Kim, M. Jazbinsek, W. Yoon, H. Yun, D. Kim, F. Rotermund and O.-P. Kwon, *Advanced Functional Materials*, 2018, 1801143.
18. P.-J. Kim, J.-H. Jeong, M. Jazbinsek, S.-J. Kwon, H. Yun, J.-T. Kim, Y. S. Lee, I.-H. Baek, F. Rotermund and P. Günter, *CrystEngComm*, 2011, **13**, 444-451.
19. J.-H. Jeong, B.-J. Kang, J.-S. Kim, M. Jazbinsek, S.-H. Lee, S.-C. Lee, I.-H. Baek, H. Yun, J. Kim, Y. S. Lee, J.-H. Lee, J.-H. Kim, F. Rotermund and O.-P. Kwon, *Scientific reports*, 2013, **3**.
20. S.-J. Kwon, O. P. Kwon, J.-I. Seo, M. Jazbinsek, L. Mutter, V. Gramlich, Y.-S. Lee, H. Yun and P. Günter, *The Journal of Physical Chemistry C*, 2008, **112**, 7846-7852.
21. B. Ruiz, Z. Yang, V. Gramlich, M. Jazbinsek and P. Günter, *Journal of Materials Chemistry*, 2006, **16**, 2839-2842.
22. G. A. Valdivia-Berroeta, L. K. Heki, E. A. McMurray, L. A. Foote, S. H. Nazari, L. Y. Serafin, S. J. Smith, D. J. Michaelis and J. A. Johnson, *Advanced Optical Materials*, 2018, 1800383.
23. S. Guan, X. Wang, Y. Li, T. Tian, G. Xu, S. Yuan and B. Cai, *Crystal Growth & Design*, 2019, **19**, 780-786.

24. G. M. Sheldrick, *Acta Crystallographica Section A: Foundations and Advances*, 2015, **71**, 3-8. Article Online
DOI: 10.1039/D07C01829E
25. P. Müller, *Crystallography Reviews*, 2009, **15**, 57-83.